

On-Wafer Optical Loss Measurements Using Ring Resonators With Integrated Sources and Detectors

Volume 6, Number 5, October 2014

E. Bitincka
G. Gilardi
M. K. Smit



DOI: 10.1109/JPHOT.2014.2352627
1943-0655 © 2014 IEEE

On-Wafer Optical Loss Measurements Using Ring Resonators With Integrated Sources and Detectors

E. Bitincka, G. Gilardi, and M. K. Smit

COBRA Research Institute, Photonic Integration Group, Department of Electrical Engineering,
University of Technology Eindhoven, 5600 MB Eindhoven, The Netherlands

DOI: 10.1109/JPHOT.2014.2352627

1943-0655 © 2014 IEEE. Translations and content mining are permitted for academic research only.

Personal use is also permitted, but republication/redistribution requires IEEE permission.

See http://www.ieee.org/publications_standards/publications/rights/index.html for more information.

Manuscript received July 7, 2014; revised August 2, 2014; accepted August 10, 2014. Date of publication August 28, 2014; date of current version September 15, 2014. This work was supported by the European FP7 project PARADIGM. Corresponding author: E. Bitincka (e-mail: e.bitincka@tue.nl).

Abstract: We demonstrate for the first time a fully integrated test structure dedicated to on-wafer propagation loss measurement. An integrated light source is used in combination with a resonant cavity and a full absorbing detector. It is fabricated in a multi project wafer run in an InP based foundry process. The probing of the integrated light source and detector with electrical signals avoids the reproducibility issues and time-overhead associated with high-precision optical alignment. The measurement accuracy, estimated to be $\sim \pm 0.2$ dB, the compact footprint (~ 1.5 mm²), and the simple and fast measurement procedure make this approach an ideal candidate for the future characterization of propagation losses in both research and manufacturing environments.

Index Terms: Waveguide devices, fabrication and characterization, semiconductor materials.

1. Introduction

Photonic integrated circuits (PICs) are becoming very widespread. Their applications range from communication technologies [1] and sensing [2] to medical diagnostics [3]. The application of the generic foundry model in photonics has radically reduced the effort to design and fabricate a Photonic IC [4], [5], but new bottle-necks at the test phase are emerging.

To determine propagation loss many methods have been proposed [6]–[8]. The Fabry-Perot method [9], [10] is used by many researchers, since its measurement accuracy is in first approximation not affected by the chip-to-fibre coupling efficiency. However, to obtain good accuracy, long samples as well as an accurate knowledge of the facet reflectivity is required. So far, the Fabry-Perot method is used with cleaved facets to form the mirrors which makes it less suitable for on-wafer testing.

Other methods include the use of a ring cavity for extracting propagation loss. In [11], the Power Transmission Ratio (PTR), defined as the ratio between the maximum and the minimum transmitted power, and the finesse of the ring over a wide range of wavelengths are measured. From these measured parameters the propagation loss and the coupling loss are determined. Another method is proposed in [12]. It estimates the overall loss, composed of propagation loss and coupling loss, from the ring PTR at different outputs.

In this work, we remove the complexity associated with the cleaving and mounting of test chips and the precision optical alignment required for loss measurement, which is present in all

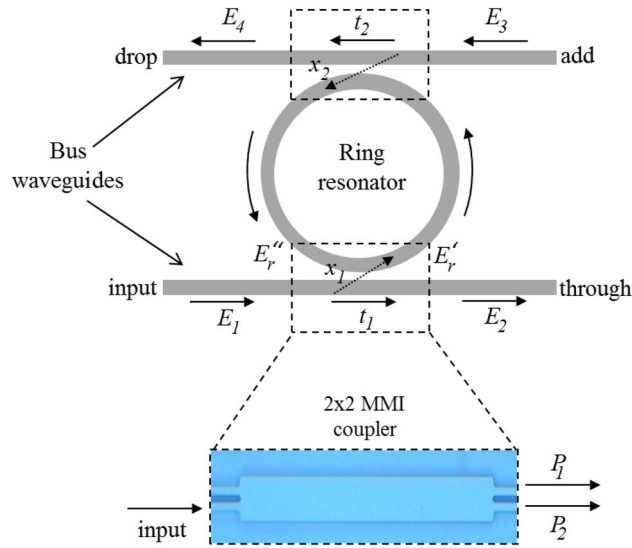


Fig. 1. Schematic of the ring resonator configuration with the 2×2 MMI coupling element shown in detail in the inset.

the above mentioned methods. We do this by implementing an electrical-only characterization method which can be performed on-wafer, before cleaving and dicing, allowing for large-scale automation and a radical step change in test-overhead.

In Section 2, we introduce a few measurement configurations and the analytical relations describing them. In Section 3, we perform an accuracy analysis of the proposed configurations. In Section 4, we present measurement results obtained by using external optical input and outputs, whereas in Section 5, fully integrated electrical measurements are reported.

2. Analytical Model of a Ring Resonator

To overcome time-consuming optical alignment, and to test the propagation loss on-wafer, i.e., before cleaving, we propose integrating of an optical cavity with a tunable light source and a detector, thus achieving on-wafer measurement. The light source and the detector are probed electrically, avoiding the critical optical coupling.

As optical cavity we choose a Ring Resonator (RR), see the schematic of Fig. 1, because of its high sensitivity to propagation loss. The input and output signals couple to the RR through the bus waveguides and the coupling element. We choose the MultiMode Interference (MMI) as coupler because of its tolerance to fabrication process and its broadband operation [13]. E_r' is the part of the input electrical field E_1 that couples to the ring. E_r'' is the part of electrical field E_r' after propagating one round trip in the ring (and eventually coupling to E_4). $t_{1,2}$ and $x_{1,2}$ are the self and cross coupling coefficients between the bus waveguide and the ring of MMI couplers 1 and 2, respectively. This ring architecture is often called the add-drop configuration.

To calculate the ring transmission the following relations as in [14], [15] are used:

$$\begin{aligned} E_1 &= 1, & E_2 &= E_1 t_1 l + E_r'' i x_1 l, & E_r' &= E_1 i x_1 l + E_r'' t_1 l \\ E_r'' &= E_r' t_2 \alpha_{ring}, & E_3 &= 0, & E_4 &= E_r' i x_2 l \sqrt{\alpha_{ring}}. \end{aligned} \quad (1)$$

In (1), the input electric field is normalized to one, whereas the input field in the add port is considered zero. α_{ring} is the attenuation experienced by the field in the ring, and l is the field attenuation coefficient due to the MMI coupler. The self and cross coupling coefficients in a lossless coupling element satisfy the following: $t = \sqrt{1 - x^2}$.

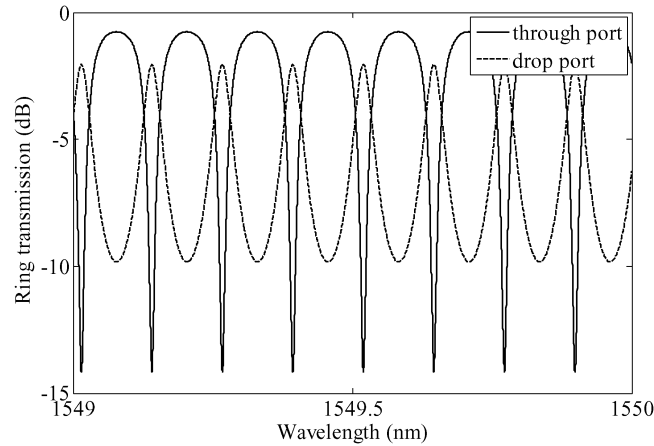


Fig. 2. Simulation of the through (solid) and drop (dashed) port transmission of a 5 mm long ring.

In the ideal case of no internal reflections inside the ring and the couplers, the output field exits only from the through and the drop port if an optical field is launched at the input port. The following transmission characteristics are obtained from the equations in (1):

$$|T_{th}|^2 = \left| \frac{E_2}{E_1} \right|^2 = \rho^2 \left[\frac{t_2^2 \tau^2 + t_1^2 - 2\tau t_1 t_2 \cos \theta}{1 + \tau^2 t_1^2 t_2^2 - 2\tau t_1 t_2 \cos \theta} \right], \quad |T_d|^2 = \left| \frac{E_4}{E_1} \right|^2 = \rho^4 \left[\frac{\tau x_1^2 x_2^2}{1 + \tau^2 t_1^2 t_2^2 - 2\tau t_1 t_2 \cos \theta} \right] \quad (2)$$

in which θ is the cumulative round trip phase and τ , defined as the round trip loss, is $\tau = \alpha_{ring} l$. In a lossless MMI coupler $l = 1$.

The integrated test structures, suitable for on-wafer measurement, are fabricated and tested in multi project wafer (MPW) runs [4]. The small footprint of these integrated test structures is of key importance when dealing with the tight space requirement present in an MPW run, and, therefore, the smallest ring perimeter is needed. The perimeter is limited by the smallest radius of the curved waveguides in InP based MPW runs ($R = 150 \mu\text{m}$), and by the MMI coupler dimensions [4] that correspond to a RR perimeter of $\sim 1.5 \text{ mm}$. The best trade-off, given the abovementioned considerations, is for rings of perimeter 1.5–5 mm, suitable for measuring the PTR over at least one FSR with a small footprint.

Several RR in this range are simulated, fabricated and measured. In Fig. 2, the simulated spectra of the through and drop port of a 5 mm long add-drop ring, calculated with Matlab are shown. The simulation considers an ideal 2×2 MMI coupler (lossless, and $P_1 = P_2$) and a waveguide propagation loss of $\alpha = 3 \text{ dB/cm}$.

The ratio between the maximum and the minimum power transmission $|T|_{\max}^2$ and $|T|_{\min}^2$ at the through port is obtained for respectively $\cos \theta = -1$ and $\cos \theta = 1$ and called the Power Transmission Ratio (PTR). A similar relation can be determined for the PTR at the drop port. Finally, there is a relation between the PTR at the through and drop port.

$$PTR_{th} = \frac{|T_{th}|_{\max}^2}{|T_{th}|_{\min}^2} = \frac{(t_1 + \tau t_2)^2 (1 - \tau t_1 t_2)^2}{(t_1 - \tau t_2)^2 (1 + \tau t_1 t_2)^2}, \quad PTR_d = \frac{|T_d|_{\max}^2}{|T_d|_{\min}^2} = \frac{(1 + \tau t_1 t_2)^2}{(1 - \tau t_1 t_2)^2}$$

$$PTR_{th} \cdot PTR_d = \left(\frac{t_1 + t_2 \tau}{t_1 - t_2 \tau} \right)^2. \quad (3)$$

The field self and cross coupling coefficients in the case of the add-drop ring configuration are $t_1 = t_2 = 1/\sqrt{2}$. The round trip loss from the through port is solved numerically and shown in Fig. 3(b). The round trip loss from the drop port and from the last equation of (3), considering

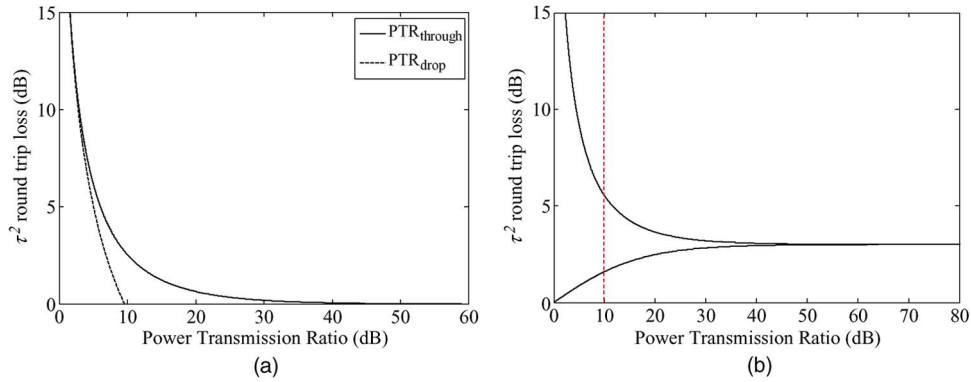


Fig. 3. Round trip loss vs. power transmission ratio for add-drop (a) and for notch ring configuration (b). The dashed vertical line represents a ring perimeter design rule which guarantees a simple way to distinguish between the “low loss” and “high loss” roots of the notch ring configuration.

only the positive roots of these equations (that have physical meaning) is given by the following relations:

$$\tau = \frac{1}{t_1 t_2} \left(\frac{\sqrt{PTR_d} - 1}{\sqrt{PTR_d} + 1} \right), \quad \tau = \frac{t_1}{t_2} \left(\frac{\sqrt{PTR_{th} \cdot PTR_d} - 1}{\sqrt{PTR_{th} \cdot PTR_d} + 1} \right). \quad (4)$$

In case only one bus is connected to the RR the simpler configuration, called notch ring, is obtained. Its transmitted spectrum and PTR are obtained from the first relation of (2) and (3) respectively, by substituting $t_1 = 1/\sqrt{2}$ and $t_2 = 1$. This RR configuration is also known as All Pass Filter (APF) since if the ring and the coupler are ideal (lossless) all the wavelengths pass through. By solving numerically τ from the PTR the graph in Fig. 3(b) is obtained.

In the notch ring configuration two different round trip losses correspond to each measured PTR, due to the quadratic equation (4). If these are on the left side of the dotted line, see Fig. 3(b), it is straightforward to select the correct propagation loss and discard the other since the ring transmission for low propagation loss has a higher quality factor compared to the one with high propagation loss. In semiconductor devices, the propagation loss value is expected to be in a narrow window, 2–4 dB/cm. A simple design rule is to choose the ring perimeter such that the measured PTR (that corresponds to this length and to typical propagation loss values) is on the left of the dotted line. The distinction between the two solutions is obvious due to the large difference in quality factor which translates into the shape of the curve. In an add-drop configuration, on the other hand, there is always a unique solution, but as shown in the next section, the add-drop configuration has a lower measurement accuracy.

3. Accuracy Analysis

By solving the first equation of (3) or (4) the round trip loss, defined as: $\tau^2 = l^2 \cdot \alpha_{ring}^2 = l^2 \cdot e^{-\alpha L}$ is measured, where α is the power attenuation coefficient. The RR perimeter L is set with high accuracy by the lithographic definition and, therefore, a known of our problem, whereas the other two parameters l and α are unknown.

3.1. Single Notch Ring Configuration

The round trip loss is composed of two contributions: a) the waveguide propagation loss α and b) the MMI excess loss l^2 . We are interested in characterizing the waveguide propagation loss but it is clear that with a single measured PTR the accurate determination of the propagation loss is closely related to our prior knowledge of the MMI excess loss. The relation

$$\Delta\alpha_l = \frac{1}{L} \frac{\partial \tau}{\partial l} \Delta l^2 \quad (5)$$

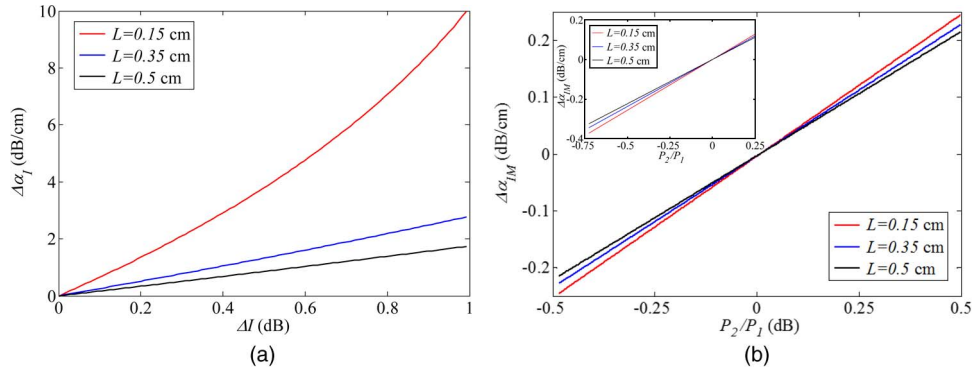


Fig. 4. Error in estimating propagation loss vs. MMI excess loss error (ΔI) (a) and MMI imbalance (b) shown for different ring perimeters and a propagation loss $\alpha = 3$ dB/cm. The inset shows the influence on $\Delta\alpha_{IM}$ of maximal imbalance of ± 0.5 dB with mean at -0.25 dB.

describes how the MMI excess loss error influences the determination of the propagation loss. In relation (5) ΔI^2 is the MMI excess loss variation, and $\Delta\alpha_I$ is the error in estimating propagation loss due to MMI excess loss variation, with the later defined as the difference between the nominal MMI excess loss and the actual MMI excess loss. A typical power loss value of 10% (0.45 dB) is used as I^2 . Relation (5), for a typical propagation loss value of $\alpha = 3$ dB/cm and several ring perimeters, is plotted in Fig. 4(a).

For a fixed value of I^2 , the higher the propagation loss experienced in the ring (longer ring perimeter and/or higher propagation loss per unit length), the smaller is the error in estimating this propagation loss. The factor $1/L$ in (5) translates $\Delta\alpha_I$ from error per round trip to error per unit length. In order to determine the propagation loss error induced by the MMI excess loss error the following procedure should be followed:

- measure the ring PTR;
- calculate the round trip loss from the first equation in (3) (or through Fig. 3(b));
- calculate the propagation loss: $\alpha = -(1/L) \cdot \ln[\tau^2/I^2]$;
- calculate $\Delta\alpha_I$ through (5).

Also the imbalance of the MMI coupler plays a role in the measurement accuracy. An imbalanced 2×2 MMI with a cross coupling coefficient of $x^2 > 0.5$ would lead to an overestimation of the propagation loss measured with the ring resonator structure and vice versa. The imbalance is defined as: $IM^2 = 10 \cdot \log_{10}(P_2/P_1)$ with P_2 and P_1 the power exiting from the two MMI outputs as shown in the inset of Fig. 1. The maximal imbalance of the 2×2 MMI in our technology is $IM^2 = \pm 0.5$ dB. To quantify the influence of the 2×2 MMI imbalance on the propagation loss calculation the following relation is used:

$$\Delta\alpha_{IM} = \frac{1}{L} \cdot (e^{-\alpha_t L} - e^{-\alpha_{t+\Delta t} L}) \quad (6)$$

where α_t and $\alpha_{t+\Delta t}$ are the propagation losses estimated, respectively, in the case of ideal and imbalanced 2×2 MMI. The factor $1/L$ in (6) translates $\Delta\alpha_{IM}$ from error per round trip to error per unit length. The influence on $\Delta\alpha_{IM}$ of maximal imbalance of ± 0.5 dB with mean at 0 dB is shown in Fig. 4(b), and with mean at -0.25 dB in the inset of Fig. 4(b). This influence is calculated for three different ring perimeters and $\alpha = 3$ dB/cm propagation loss.

Since the MMI excess loss and the imbalance are independent on each other the overall propagation loss measurement accuracy attainable with the notch ring configuration is [16]

$$\Delta\alpha = \sqrt{\Delta\alpha_I^2 + \Delta\alpha_{IM}^2} \quad (7)$$

The excess loss induced error dominates the overall error.

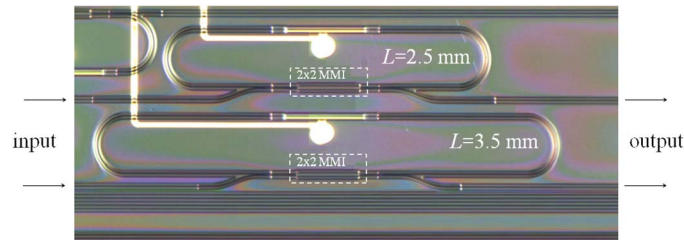


Fig. 5. Microscope photo of notch rings.

Fig. 4(b) shows the effect of a spread in imbalance from -0.5 dB to $+0.5$ dB. For a systematic offset of -0.25 dB the same range of imbalance becomes -0.75 dB to $+0.25$ dB as shown in inset of Fig. 4(b). Considering the worst case scenario of max imbalance the imbalanced induced error goes from ~ 0.25 dB/cm to ~ 0.3 dB/cm. This difference is negligible when compared to MMI excess loss induced errors $\Delta\alpha_I$; see Fig. 4(a).

3.2. Add-Drop Ring Configuration

In the case of an add-drop ring configuration there is the contribution of two 2×2 MMI couplers in each round trip. Therefore, the contribution of the ΔI and the IM in the round trip loss, experienced by the field and estimated by the PTR at the through and at the drop port, is twice as large as in the notch ring configuration. The propagation loss measurement uncertainty attainable with the add-drop ring is

$$\Delta\alpha = \sqrt{(2 \cdot \Delta\alpha_I)^2 + (2 \cdot \Delta\alpha_{IM})^2}. \quad (8)$$

From the measurement accuracy point of view we can state that the notch ring is twice as good as the add-drop ring for a given footprint. The add-drop ring in turn has a unique PTR for any given round trip loss.

3.3 Double Notch Ring Configuration

The last configuration that we consider is the double notch ring with different perimeters and same coupling element. With this configuration we can discriminate between propagation loss and MMI excess loss by assuming that the MMI couplers have the same properties (excess loss and imbalance).

If the RRs are in the same chip area, as those in Fig. 5, only the difference in excess loss and imbalance of the corresponding MMIs plays a role in the measurement accuracy. If the MMIs are closely spaced in the PIC their excess loss and imbalance vary with less than 4%. This value was measured through a dedicated test structure composed of an odd number of cascaded 2×2 MMI couplers. The total imbalance of a cascaded number of 2×2 MMIs scales up in first approximation linearly if compared to that of a single 2×2 MMI, thus making it possible to measure. The final accuracy is calculated by using (7). The singular ΔI^2 and IM^2 uncertainty contributions are still calculated using (5) and (6) with the value of 4% measured for MMIs closely spaced in PIC.

If a single notch ring is used than the more realistic ΔI^2 and IM^2 of 0.1 should be used.

4. Optical Experiments

The test structures presented in this section are designed according to a generic integration concept, using standardized building blocks, and it is fabricated in a MPW run of the COBRA platform [4]. We verify the validity of the analytical models derived in Section 2, and the measurement accuracy developed in Section 3 for the best ring configurations in terms of measurement accuracy, namely the notch ring, and the double notch ring configurations, using test structures without integrated light source and detector.

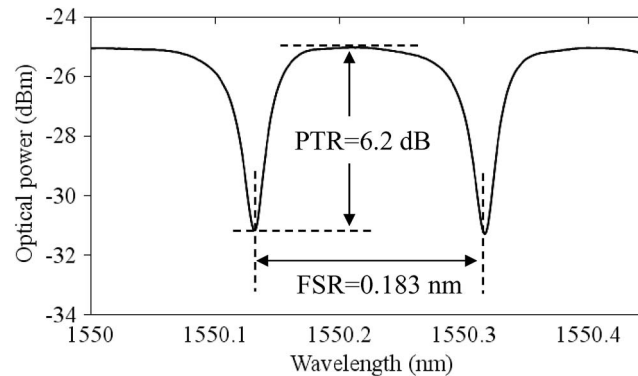


Fig. 6. Transmission measurement, Power Transmission Ratio, and Free Spectral Range of a 3.5 mm long racetrack in the notch ring.

All the ring configurations that we measure in this section and the next one have the shape of a racetrack, as shown in Fig. 5, which means that they are composed of 2 semi-circular arcs of π radians connected by straight waveguides. The analytical model and the accuracy analysis presented in the previous sections are not dependent on the ring shape but on the ring perimeter, thus the previous analysis is still valid for a racetrack shape ring. Moreover, the use of the racetrack allows the decoupling of the ring radius from the ring perimeter.

The waveguide structure of the COBRA foundry process consists of a $0.5 \mu\text{m}$ Q1.25 waveguide layer between an InP top and bottom cladding layer. Q1.25 means lattice-matched quaternary material (InGaAsP) with a composition such that the band edge is at a wavelength of $1.25 \mu\text{m}$. The deep etched waveguides are etched $> 100 \text{ nm}$ into the lower cladding layers [4]. All the straight and curved waveguides are designed to be $1.5 \mu\text{m}$ wide and deeply etched for allowing small bending radii and, therefore, a compact RR. The $1.5 \mu\text{m}$ wide waveguides are single mode, and thus, possible higher order modes, excited in junctions or imperfections, should not be guided.

4.1. Notch Ring Configuration

Fig. 6 shows the measured spectrum of the 3.5 mm long ring shown in Fig. 5. To suppress the back reflections from the facets the input and output waveguides that exit the chip were designed at a 7° angle. No evidence of facet reflections in the ring transmission was found.

The passive ring configurations have been measured using an Agilent HP 8168A tuneable source connected to a polarization controlling stage and a lensed single-mode polarization-maintaining fibre. Transverse Electric (TE) light was coupled to the input bus waveguide of the ring cavity. Light was coupled out of the bus waveguide through a lensed fibre, and finally fed to the power meter with a noise floor $< -60 \text{ dBm}$. A wavelength sweep was performed with a step of 1 pm and the recorded power is shown in Fig. 6.

To determine $\Delta\alpha_l$ we repeat the procedure with (in brackets) the values that apply to the single notch ring configuration under examination:

- measure ring PTR (6.2 dB);
- determine the round trip loss through (3) (or Fig. 3(b)): $\tau^2 = 0.785(1.05 \text{ dB})$;
- calculate the propagation loss: $\alpha = 0.39 \text{ cm}^{-1}(1.7 \text{ dB/cm})$;
- calculate the propagation loss error through (5) $\Delta\alpha_l = 0.25(1.25 \text{ dB/cm})$.

Relation (5) gives the differential error done when approximating a function with its first derivative calculated around the point $\alpha = 1.7 \text{ dB/cm}$ (0.39 cm^{-1}) for an MMI excess loss error of $\Delta l^2 = 0.1$.

By following the same procedure for the MMI imbalance described in the previous section the propagation loss error for the nominal MMI imbalance is $\Delta\alpha_{MM} = 0.032$ (0.13 dB/cm).

The final measurement accuracy using (7) is $\Delta\alpha = 0.252$ (1.26 dB/cm), and the measured propagation loss is $\alpha = 1.7 \pm 0.63 \text{ dB/cm}$.

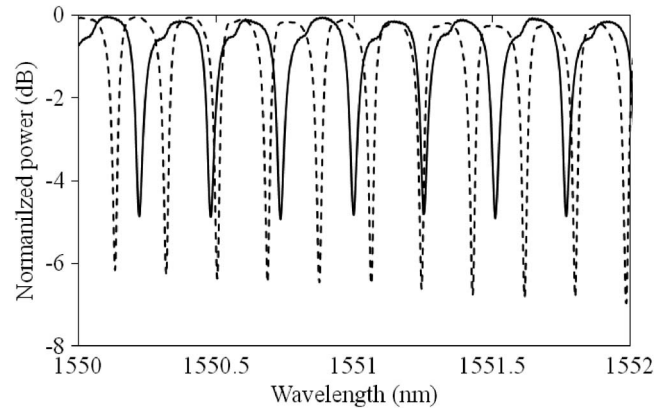


Fig. 7. Measured transmission spectra of a 2.5 mm long ring (solid), and of a 3.5 mm long ring (dashed).

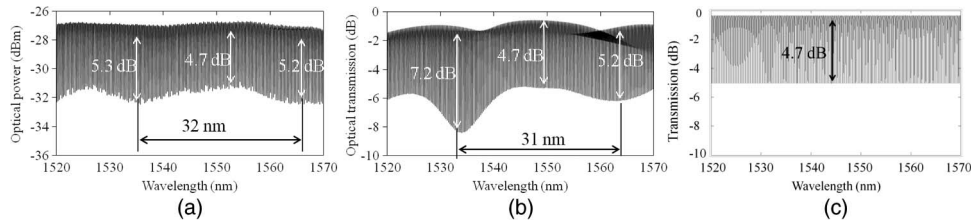


Fig. 8. Measured transmission of a 2.5 mm long ring is shown (a). A simulated transmission is shown that considers the propagation of fundamental and higher order modes (b) and when only fundamental TE mode is present (c). The MMI excess loss was included in the simulation.

4.2 Double Notch Ring Configuration

To cancel the inaccuracy due to the 2×2 MMI coupler we use two rings with the same 2×2 MMI coupler but different overall length. The first ring is the one previously analyzed ($L_1 = 0.35$ cm), whereas the second has a length $L_2 = 0.25$ cm. Thanks to the racetrack configuration the difference in length is implemented in the straight waveguide section and, therefore, gives us a measurement of the propagation loss in straight waveguide, see Fig. 5. The transmission of the two rings is shown in Fig. 7. The power transmission ratios are $\text{PTR}_1 = 6.2$ dB and $\text{PTR}_2 = 4.7$ dB respectively, which by solving (3) for the notch ring or by using Fig. 3(b), corresponds to $\tau_1^2 = 0.785$ (1.05 dB) and $\tau_2^2 = 0.83$ (0.81 dB) round trip loss. Knowing the ring length difference $\Delta L = 0.1$ cm it is straight forward to calculate the propagation loss $\alpha = 1/\Delta L \cdot \ln(\tau_1^2/\tau_2^2) = 0.56$ cm⁻¹ (2.4 dB/cm), which corresponds to an MMI excess loss of $I^2 = \tau_{1,2}^2/\alpha_{ring_{1,2}}^2 = 0.955$ (0.2 dB). In this calculation, we assumed that the propagation loss experienced in the straight and curved waveguides is the same. Taking into account the excess loss variations and imbalance of adjacent MMIs, $\Delta I^2 = 0.04$ and $IM^2 = 0.04$ as described in Section 3.3, the double sided accuracy interval becomes $\Delta\alpha = 0.1$ (0.45 dB/cm). The measured propagation loss is $\alpha = 2.4 \pm 0.23$ dB/cm.

In the ring transmission a slight modulation of the fringes can be seen. This modulation is due to more than one mode propagating in the circuit with different propagation constants. These modes are either the two polarizations or higher order modes. To investigate the possibility of higher order mode excitation a long wavelength sweep measurement was performed for the 2.5 mm long ring of Fig. 5. This measurement is compared to the simulation when considering higher order modes propagating in the circuit; see Fig. 8.

The measured and the simulated transmission match well in terms of the beating period (~ 32 nm) which confirms that the observed modulation is caused by a higher order mode, in

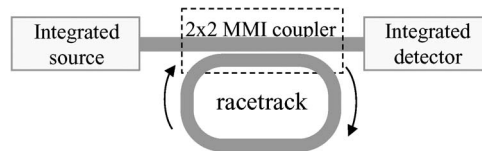


Fig. 9. Schematic of the ring based test structure for measuring propagation loss.

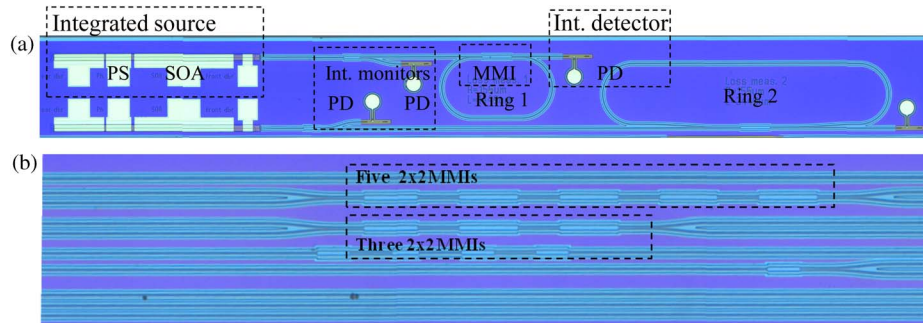


Fig. 10. (a) Fully integrated notch ring resonator structure for propagation loss measurement, and (b) the dedicated test structure for measuring excess and imbalance loss for closely spaced 2×2 MMIs.

this case the first order mode. The problem of higher order modes and/or the TM polarization excitation is solved in the on-wafer test structure that includes an integrated single mode laser source that is presented in the next section.

The simulation was performed using the Agilent's Advanced Design Systems (ADS) circuit simulator tool with custom plug-ins to support photonic waveguides.

To verify the propagation loss measurement result the Fabry-Perot method [11], [12] was used in a straight deeply etched referenced waveguide. Propagation loss of $\alpha = 2.35$ dB/cm was measured for a 3.2 mm long cavity and a simulated facet reflectivity of $R = 0.31$. This propagation loss is in very good agreement with the result of the double notch configuration.

5. Electrical Experiments

The last test structures presented in this section and shown in the schematic of Fig. 9 concern the notch ring coupled through a 2×2 MMI to an integrated tunable laser source and an integrated photo detector are designed according to a generic integration concept, using standardized building blocks, and it is fabricated in a MPW run at the Oclaro platform [4].

The measured notch rings have perimeters of 1.44 mm (the smallest possible when complying with the minimum radius of curved waveguides, $150 \mu\text{m}$, and MMI length of $150 \mu\text{m}$) and 3.44 mm long (2 mm longer than ring 1), as shown in Fig. 10.

The integrated source for these test structures is a tunable Distributed Bragg Reflector (DBR) laser [1]. The output signal is measured by an integrated fully absorbing PD. To get an interference pattern at the ring resonator output the wavelength of the source should be tunable. The DBR laser configuration used is the standard one offered by the foundry. The measured transmission of the 1.44 mm and 3.44 mm long rings is shown in Fig. 11(a). The output power, measured at the integrated detector, is normalized with the power measured at the integrated monitor. The monitor is used to track the laser output power which drops by few dB during tuning.

The Semiconductor Optical Amplifier (SOA) section of the DBR laser was constantly pumped right above threshold. Higher pumping currents were avoided to lower the noise floor. The lasing wavelength was tuned by varying the current applied at the laser Phase Section (PS), thus only a limited continuous tuning between two consecutive longitudinal Fabry-Perot modes is obtained. The DBR mirrors were not tuned to avoid mode hops and to simplify the continuous

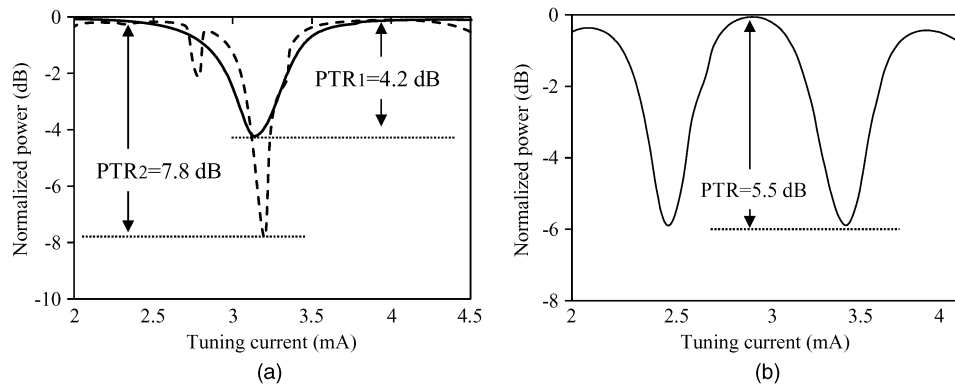


Fig. 11. Measured transmission of a 1.44 mm long (solid) and of a 3.44 mm long (dashed) ring resonator (a) and of a 5.2 mm long ring resonator high loss MPW run wafer (b). The current applied at the phase section of the DBR lasers is used to fine tune its wavelength. The smallest dip in ring 2 transmission (dashed line) is due to laser mode hop.

wavelength tuning procedure (no second control signal applied to the DBR mirror). The small tuning window (~ 0.45 nm), with a careful design of the RR perimeter, is sufficient to obtain a wavelength sweep over one FSR for ring 1. The power at the output is measured by an integrated full absorbing photo detector.

The measured power transmission ratios are $\text{PTR}_1 = 4.2$ dB and $\text{PTR}_2 = 7.8$ dB, which, by solving (3) for the notch ring or by using Fig. 3(b), correspond to $\tau_1^2 = 0.846$ (0.73 dB) and $\tau_2^2 = 0.743$ (1.3 dB) round trip loss respectively. Considering the ring length difference $\Delta L = 0.2$ cm it is straight forward to calculate the propagation loss $\alpha = 1/\Delta L \cdot \ln(\tau_1^2/\tau_2^2) = 0.65$ cm^{-1} (2.82 dB/cm). This propagation loss corresponds to an MMI excess loss of $I^2 = \tau_{1,2}^2/\alpha_{ring_{1,2}}^2 = 0.929$ (0.32 dB). In this calculation we assumed that the propagation loss experienced in the straight and curved waveguides is the same.

A dedicated test structure for measuring excess loss and imbalance of 2×2 MMIs was included in the chip, see Fig. 10(b). The excess loss of the 2×2 MMI, measured on these test structures was found to be in the range 0.3–0.5 dB over the C-band which is in good agreement with the results obtained by the RRs. For the imbalance the measurement showed 0.1–0.2 dB. Taking into account these values for the excess loss and imbalance of adjacent MMIs, $\Delta I^2 = 0.04$ and $IM^2 = 0.04$, the accuracy becomes $\Delta\alpha = 0.1$ (0.45 dB/cm). So the final measured propagation loss is $\alpha = 2.82 \pm 0.23$ dB/cm.

The integrated monitor and the integrated output detector are used for a relative measurement of the power of the integrated tunable laser, therefore, no absolute calibration of the splitting MMI or of the monitor detector is needed.




A similar test structure was present in a wafer that due to some processing problems suffered high losses. Nonetheless the integrated RR of a perimeter of 5.2 mm (four times larger than the smallest ring perimeter possible), under the same working conditions as the one previously described, showed a PTR of 5.5 dB which corresponds to 1 dB/cm or 15.5 dB/cm propagation loss depending whether we are on the lower or higher side of the critical coupling. From the low quality factor of the ring transmission [see Fig. 11(b)], the 1 dB/cm propagation loss was discarded. This example shows the versatility of the integrated ring resonator test structure in measuring propagation loss over a large range.

To test the method the structure was proposed in different MPW runs from different foundries (Optical experiments at COBRA and Electrical experiments at Oclaro MPW run). The measured values agree well with the typical values reported by these foundries and estimated by other propagation loss measurement method as the Fabry-Perot one.

In Table 1, a comparison of the RR configurations in terms of footprint and measurement accuracy for a typical ring perimeter of 0.25 cm and loss $\alpha = 3$ dB/cm is shown. The best

TABLE 1

Comparative table of the principle ring configuration. The three configurations use the same 2×2 MMI coupler

	<i>Single notch</i>	<i>Double notch</i>	<i>Add-drop</i>
			
Measured accuracy (dB/cm)	± 0.55	± 0.22	± 1.3
Footprint RR (mm^2)	1.0	1.5	1.0

configuration in terms of accuracy is the double notch ring, whereas in terms of footprint the single notch and the add-drop are better. A considerable part of the footprint is due to the integrated DBR laser, see Fig. 10(a). The gain in terms of measurement accuracy obtained with the double notch ring is several times larger than with the other methods with only a small price in footprint. Therefore, this is our method of choice for on-wafer propagation loss determination.

In the single notch configuration two propagation loss values correspond to every measured PTR. Data interpretation is needed to choose the correct propagation loss. In the double notch configuration two values of the propagation loss correspond to each of the rings but only two of the solutions are consistent. The add-drop configuration has only one solution for any measured PTR.

6. Conclusion

We demonstrated for the first time on-wafer propagation loss measurements by integrating a tunable light source, a photo detector, and a ring cavity. The test structure was fabricated in an MPW run in an InP-based foundry process. This measurement method uses electrical probing rather than optical alignment of lensed fibers and is, therefore, faster and more reproducible. It can be carried out with a current and a voltage source avoiding expensive equipment such as optical spectrum analyzers, tunable lasers and power meters and, moreover, it can be done earlier in the PIC processing, i.e. before cleaving the wafer. Experimental data show that this method is consistent with other classical methods as, for example, the Fabry-Perot measurement method. It can be applied to measure propagation loss from 1–2 dB/cm to 20 dB/cm or higher. An accuracy analysis was carried out for different ring configurations. The analysis identified the MMI excess loss error and MMI imbalance as the main factors influencing propagation loss measurement accuracy. The accuracy is dependent on the ring configuration and the propagation loss. The best ring configuration in terms of accuracy is the double notch ring, $\Delta\alpha = \pm 0.23$ dB/cm. Its results are comparable to the Fabry-Perot. The Fabry-Perot method depends on prior knowledge of the facet reflectivity, and it requires cleaved facets and optical alignment. All draw-backs are removed with our integrated measurement approach.

Acknowledgement

Oclaro is acknowledged for fabricating the integrated test structures. The Fraunhofer Heinrich Hertz Institute in Berlin is acknowledged for the experience and knowledge on integrated tunable laser provided to the author.

References

- [1] A. Ward *et al.*, "Widely tunable DS-DBR laser with monolithically integrated SOA: Design and performance," *IEEE J. Sel. Topics Quantum Electron.*, vol. 11, no. 1, pp. 149–156, Jan./Feb. 2005.

- [2] X. Fan and I. White, "Optofluidic Microsystems for chemical and biological analysis," *Nat. Photon.*, vol. 5, no. 10, pp. 591–597, Oct. 2011.
- [3] V. Nguyen *et al.*, "Spectral domain optical coherence tomography imaging with an integrated optics spectrometer," *Opt. Lett.*, vol. 36, no. 7, pp. 1293–1295, Apr. 2011.
- [4] M. Smit *et al.*, "An introduction to InP-based generic integrated technology," *Semicond. Sci. Technol.*, vol. 29, no. 5, pp. 41, Jun. 2014.
- [5] G. Gilardi and M. Smit, "Generic InP-based integration technology: Present and prospects," *Progr. Electromagn. Res.*, vol. 46, pp. 23–35, Jun. 2014.
- [6] Y. Okamura, S. Yoshinaka, and S. Yamamoto, "Measuring mode propagation losses of integrated optical waveguides: A simple method," *Appl. Opt.*, vol. 22, no. 23, pp. 3892–3894, Dec. 1983.
- [7] P. Brannon, "Improved method of measuring optical waveguide propagation losses," *Appl. Opt.*, vol. 25, no. 20, pp. 3596–3597, Jun. 1986.
- [8] A. Rickman, G. Reed, B. Weiss, and F. Namavar, "Low-loss planar optical waveguides fabricated in SIMOX material," *IEEE Photon. Technol. Lett.*, vol. 4, no. 6, pp. 633–635, Jun. 1992.
- [9] R. Walker, "Simple and accurate loss measurement technique for semiconductor optical waveguides," *Electron. Lett.*, vol. 21, no. 13, pp. 581–583, Jun. 1985.
- [10] B. Hakki and T. Paoli, "CW degradation at 300 oK of GaAs double-heterostructure junction lasers. II. Electronic gain," *J. Appl. Phys.*, vol. 44, no. 9, pp. 4113–4119, May 1973.
- [11] W. McKinnon *et al.*, "Extracting coupling and loss coefficients from a ring resonator," *Opt. Exp.*, vol. 17, no. 21, pp. 18 971–18 982, Oct. 2009.
- [12] F. Xia, L. Sekaric, and Y. Vlasov, "Mode conversion losses in silicon-on-insulator photonic wire based racetrack resonators," *Opt. Exp.*, vol. 14, no. 9, pp. 3872–3886, Apr. 2006.
- [13] L. Soldano, "Optical multi-mode interference devices based on self-imaging : Principles and applications," *J. Lightw. Technol.*, vol. 13, no. 4, pp. 615–627, Apr. 1995.
- [14] A. Yariv, "Universal relations for coupling of optical power between microresonators and dielectric waveguides," *Electron. Lett.*, vol. 36, no. 4, pp. 321–322, Feb. 2000.
- [15] A. Vörckel, M. Mönster, W. Henschel, P. Bolivar, and H. Kurz, "Asymmetrically coupled silicon-on-insulator microring resonators for compact add-drop multiplexers," *IEEE Photon. Technol. Lett.*, vol. 15, no. 7, pp. 921–923, Jul. 2003.
- [16] J. R. Taylor, *An Introduction to Error Analysis: The Study of Uncertainties in Physical Measurements*. Sausalito, CA, USA: University Science, 1982.